

# Split-pulse X-ray photon correlation spectroscopy with seeded X-rays from X-ray laser to study atomic-level dynamics

Yuya Shinohara<sup>1\*</sup>, Taito Osaka<sup>2</sup>, Ichiro Inoue<sup>2</sup>, Takuya Iwashita<sup>3</sup>, Wojciech Dmowski<sup>4</sup>, Chae Woo Ryu<sup>4</sup>,  
Yadu Sarathchandran<sup>5</sup>, Takeshi Egami<sup>1,4,5</sup>

<sup>1</sup>*Materials Science and Technology Division, Oak Ridge National Laboratory, Oak Ridge, Tennessee  
37831, USA*

<sup>2</sup>*RIKEN SPring-8 Center, Sayo, Hyogo 679-5198, Japan*

<sup>3</sup>*Department of Integrated Science and Technology, Oita University, Dannoharu, Oita 870-1192, Japan*

<sup>4</sup>*Department of Materials Science and Engineering, The University of Tennessee, Knoxville, Tennessee,  
37996 USA*

<sup>5</sup>*Department of Physics and Astronomy, The University of Tennessee, Knoxville, Tennessee, 37996 USA*

## Notice of Copyright

This manuscript has been authored by UT-Battelle, LLC under Contract No. DE-AC05-00OR22725 with the U.S. Department of Energy. The United States Government retains and the publisher, by accepting the article for publication, acknowledges that the United States Government retains a non-exclusive, paid-up, irrevocable, worldwide license to publish or reproduce the published form of this manuscript, or allow others to do so, for United States Government purposes. The Department of Energy will provide public access to these results of federally sponsored research in accordance with the DOE Public Access Plan (<http://energy.gov/downloads/doe-public-access-plan>).

**With their unprecedented brilliance and temporal structure, X-ray free-electron laser can unveil atomic-scale details of ultrafast phenomena. Recent progress in split-and-delay optics (SDO), which produces two X-ray pulses with time-delays, offers bright prospects for observing dynamics at the atomic-scale. However, their insufficient pulse energy has limited its application either to phenomena with longer correlation length or to measurement with a fixed delay-time. Here we show that the combination of the SDO and self-seeding of X-rays increases the pulse energy and makes it possible to observe the atomic-scale dynamics in a timescale of picoseconds. We show that the speckle contrast in scattering from water depends on the delay-time as expected. Our results demonstrate the capability of measurement using the SDO with seeded X-rays for resolving the dynamics in temporal and spatial scales that are not accessible by other techniques, opening new opportunities for studying the atomic-level dynamics.**

Since the observation of X-ray speckles using coherent X-rays,<sup>1</sup> scientists have developed a speckle-based technique called X-ray Photon Correlation Spectroscopy (XPCS), where the temporal correlation of speckle patterns is used to extract dynamics of materials at specific correlation lengths.<sup>2-5</sup> Earlier XPCS studies using synchrotron X-rays primarily focused on determining dynamics on relatively longer length-scales ( $> 10$  nm).<sup>6-11</sup> Only a few studies have recently been carried out at the atomic-scales although the timescale is limited to a relatively slow dynamics ( $> 10$  s).<sup>12-14</sup> Extending the timescale of XPCS to picoseconds, which are relevant to studying the atomic-level dynamics in matter such as liquid, has been challenging because of the insufficient intensity of coherent X-rays and the limited frame-rate of detectors (typically  $< 1$  kHz). Meanwhile, recent progress in high-energy-resolution inelastic X-ray and

neutron scattering has extended their accessible timescale and its applications.<sup>15,16</sup> Nevertheless, their timescale and length-scale are not appropriate for probing the atomic-level dynamics in a wide timescale of picoseconds to nanoseconds due to the limitation in energy resolution and intensity. Accordingly, the atomic-level dynamics in liquids, particularly supercooled liquids, remains elusive.

The advent of X-ray free electron lasers (XFELs),<sup>17,18</sup> together with recent progress in split-and-delay optics (SDO),<sup>19,20</sup> has raised the expectation for bridging the aforementioned gap by extending the timescale of XPCS to picoseconds.<sup>21</sup> In this timescale, measuring the time-correlation of each speckle is not practical because of the intrinsic limitation on the temporal resolution of X-ray detectors as well as the repetition rate of the XFELs. This limitation is overcome by a split-and-delay approach,<sup>21,22</sup> which uses two X-ray pulses that are generated from a single XFEL pulse. The accessible timescale is determined by the ability to generate two pulses separated in time  $\Delta t$ . The contrast  $\beta(Q, \Delta t)$  at momentum transfer  $Q$  in the sum of speckle scattering patterns from a sequence of two separate X-ray pulses is analyzed to extract the information on dynamics by the Speckle Visibility Spectroscopy (SVS),<sup>23,24</sup> utilizing the relationship between  $\beta(Q, \Delta t)$  and the intermediate scattering function,  $f(Q, \Delta t)$ .<sup>20,22,25–27</sup> Recently SVS using X-ray pulses with variable pulse duration has been demonstrated for the femtoseconds dynamics in supercooled water without using SDOs,<sup>28</sup> and accelerator-based double X-ray pulse generations<sup>29,30</sup> are also accomplished; however, their pulse-duration or time-delay is restricted either to a limited range of orders of femtosecond or to discrete steps of hundreds of picoseconds. Alternatively, in an SDO system, a single XFEL pulse is divided into two pulses by a beam splitter, and a delay-time between the pulses is controlled by their path length difference. Hard X-ray SDO systems have hitherto been developed,<sup>19,31–34</sup> and a few

experimental results using the SDO have been reported.<sup>20,35</sup> However, their application was still limited to a longer length-scale ( $> 1$  nm) and the study of atomic-level dynamics at sub-nm scale using X-ray SVS with an SDO has not been reported because of the insufficient pulse energy of X-rays.

Here we report the first X-ray SVS result utilizing the SDO combined with the self-seeded X-rays<sup>36</sup> at SPring-8 Angstrom Compact free-electron Laser (SACLA).<sup>18</sup> The self-seeding of X-rays<sup>36-38</sup> generates narrow-band X-rays and thus can provide higher X-ray intensity after passing through the SDOs. The increase in the X-ray pulse energy at the sample position enables the application of XSVS at high  $Q$  ( $> 1 \text{ \AA}^{-1}$ ), which is relevant to the study of atomic-level dynamics.

## Results

**X-ray scattering of water using the SDO and seeded X-rays.** The XSVS experiment was carried out using the setup shown in Fig. 1. A reflection self-seeding<sup>36</sup> at a photon energy of 10 keV was employed. Each X-ray pulse was then split into two sub-pulses using a wavefront-division SDO, making use of Si(220) crystals.<sup>31</sup> The delay-time  $\Delta t$  between the sub-pulses was controlled by the path length difference between the variable-delay branch and the fixed-delay branch. We changed  $\Delta t$  between 0 and 2 ps, although the accessible range of  $\Delta t$  is much longer.<sup>31</sup> The pulse energy of the variable-delay branch ( $I_{\text{high}}$ ) and the fixed-delay branch ( $I_{\text{low}}$ ) were monitored by the beam intensity monitors.<sup>39</sup> The exit beams were overlapped and focused to a size of 0.7  $\mu\text{m}$  (H) and 0.9  $\mu\text{m}$  (V) at the sample position with X-ray mirrors.<sup>40</sup>

Figure 2a shows the histogram of X-ray pulse energy at the sample position,  $I_{\text{tot}} = I_{\text{high}} + I_{\text{low}}$ . The dashed line is a fit to the experimental data using a gamma density distribution function:<sup>41</sup>

$$P(I_{\text{tot}}) = \left( \frac{M}{\langle I_{\text{tot}} \rangle} \right)^M \frac{\exp(-MI_{\text{tot}}/\langle I_{\text{tot}} \rangle) I_{\text{tot}}^{M-1}}{\Gamma(M)},$$

where  $\Gamma(M)$  is the gamma function and  $\langle \dots \rangle$  represents the average over shots.  $M$  is the number of modes. Our analysis yields  $M = 2.24$  with  $\langle I_{\text{tot}} \rangle = 7.7 \mu\text{J}$ . The energy bandwidth of single-shot self-seeded X-ray ( $\sim 2 \text{ eV}$  in FWHM) improved the throughput of the SDO system, compared to the case using only self-amplified spontaneous emission (SASE), where the averaged bandwidth is around  $30 \text{ eV}$ .<sup>31</sup> This significant improvement facilitates the XSVS at high  $Q$ . The split ratio,  $R = I_{\text{low}}/(I_{\text{low}} + I_{\text{high}})$ , was distributed shot-by-shot, and 13% of the total events satisfy the condition of the ratio of  $0.475 < R < 0.525$  (Fig. 2b). This distribution originated from shot-to-shot variations in the profile and position of the incident X-ray beam.

In our experiment, a continuous stream of water with a flow rate of  $0.7 \text{ mL/min}$  was irradiated by the X-rays. The diameter of the water stream was  $50 \mu\text{m}$ , much larger than the variation in the beam position at the sample during the experiment, as shown in Fig. 2c. The scattering from the sample was recorded by three multi-port charge-coupled devices (MPCCDs)<sup>42</sup> located  $1 \text{ m}$  downstream of the sample to cover  $Q$ -ranges shown in Fig. 3. The speckle size is estimated to be around  $0.18 \text{ mm}$ , which is larger than the pixel size of the MPCCDs,  $50 \mu\text{m}$ .

Figure 3 shows a one-dimensional scattering intensity profile, which was averaged over  $29,051$  shots, the averaged pulse energy of which was  $7.3 \mu\text{J}$ . A droplet algorithm<sup>43</sup> was employed to convert raw data into the digitized X-ray photon images. The number of photons at each pixel per shot was  $0.7$  times the estimated value that was calculated using the result of high-

energy X-ray diffraction.<sup>44</sup> This discrepancy could originate from additional absorption by Kapton windows of the helium chambers and air along the path. The result shows that the observed X-ray intensities predominantly represent scattering from the water.

**Speckle contrast analysis.** From the statistics of observed photons, the visibility of the X-ray speckle pattern at specific  $Q$  was calculated. Following the previous studies,<sup>20,27,28,35,43</sup> we assume that the probability for observing  $k$  photons at a single-pixel is described by a negative binomial distribution with the average number of photons per pixel,  $\mu$ , when the number of scattered photons is low:<sup>41</sup>

$$P(k|\mu, M_s) = \frac{\Gamma(k + M_s)}{\Gamma(M_s)k!} \left(\frac{M_s}{M_s + \mu}\right)^k \left(\frac{\mu}{M_s + \mu}\right)^{M_s}.$$

Here  $M_s$  is the number of modes in observed scattering images and is related to  $\beta$  such that  $\beta = 1/M_s$ .<sup>20,22,43</sup> By using the log-likelihood ratio statistic of this distribution, the value of  $M_s$  was determined as demonstrated in earlier studies<sup>20</sup> as shown in Fig. 4. At  $Q = 2 \text{ \AA}^{-1}$ , as the delay-time increased, the visibility of speckle reduces, reflecting the dynamics of the sample. At delay-times longer than  $\Delta t = 1.0 \text{ ps}$ , the values of  $\beta$  agree with that of the uncorrelated beams without spatial overlap. The decrease in the contrast is comparable to those calculated from the result of inelastic X-ray scattering of water as shown in Fig. 4.<sup>45,46</sup> This is the first time that the dependence of the speckle contrast on the delay-time was measured using an SDO system. On the other hand, we could not find a clear decaying behavior at  $Q = 3 \text{ \AA}^{-1}$  or higher, presumably due to the smaller number of photons and the additional decoherence at a higher  $Q$ , which will be addressed in a future study.

## Discussion

The estimated values of  $M_s$  depend on (1) the dynamics of the sample to be obtained, (2) the splitting ratio  $R$ , (3) the initial contrast, (4) the contrast reduction due to the experimental setting, and (5) the degree of decoherence between the two split pulses.<sup>20,22</sup> In this letter, we did not include the data with  $|R - 0.5| > 0.025$  to reduce the uncertainty with respect to (2). We can reasonably assume that the sample thickness involved in the scattering was constant because the shot-by-shot positional fluctuations of X-rays were small (Fig. 2c). Then, the effects of (3) and (4) can be expressed in terms of  $\beta$ , which was estimated to be  $\beta_0 = 0.23 \pm 0.02$  at  $Q = 2 \text{ \AA}^{-1}$  by measuring the contrast with a single pulse using the fixed-delay branch. This value is consistent with the baseline value, because the baseline should be  $\beta_0/2$ .<sup>20</sup> Meanwhile, the result for dual pulses was  $\beta(Q, \Delta t = 0) = 0.14$ , smaller than  $\beta_0$ . This contrast reduction can be reasonably explained by the degree of decoherence between the sub-pulses. The angular mismatch between the sub-pulses,<sup>47</sup> 150 mrad, creates the positional difference between two speckles  $\sim 0.15$  mm on the detector plane, thereby reducing the contrast from 0.23 to  $\sim 0.15$ . Remaining discrepancy could originate from shot-to-shot incomplete geometrical overlap of the sub-pulses.<sup>20</sup> The relative positional fluctuations were inherently random as shown in the lower rows of Fig. 2c and cannot be monitored simultaneously during the X-ray SVS measurement. Including these effects in analyses to provide reasonable estimates of decoherence using more sophisticated approaches such as hierarchical models<sup>48</sup> warrant future studies. The use of hierarchical models will also allow us to include the data with different  $R$  for the estimation, thereby significantly increasing the statistics. This will make it possible to extract meaningful information at higher  $Q$  and could facilitate the evaluation of femtoseconds to nanoseconds dynamics at the atomic scale.

## Methods

**Self-seeded X-rays.** We used an 8-GeV electron beam with a charge of 130 pC and  $\sim 10$  fs duration for reflection self-seeding using a Si(220) microchannel-cut crystal monochromator at SPring-8 Angstrom Compact free-electron Laser (SACLA)<sup>18</sup> as described in ref.<sup>36</sup> Eight undulator segments were used to generate the SASE with average pulse energy of 80  $\mu$ J, and a channel-cut crystal monochromator was used to select a 10 keV radiation with a bandwidth of 0.6 eV (FWHM). The X-ray was used as a seed, which was amplified by the 13 downstream undulator segments.

**Split-and-delay optics.** A wavefront-division SDO using Si(220) crystals was used to split a single pulse into two sub-pulses with a delay time.<sup>31</sup> The SDO system was installed 70 m downstream from the last undulator segment. Shot-to-shot noninvasive diagnostics of pulse energies for both branches were made using inline diagnostic modules. After propagating through the SDO, the pulse width of X-ray was  $\sim 8$  fs, which was similar to that of SASE (6-8 fs).

**Experimental Setting.** The experiment was carried out at BL3, SACLA (Japan). The exit beams from the SDO system were focused on a sample position with a focusing mirror system and hit a water jet. The diameter of the water jet was 50  $\mu$ m, and the water temperature was 22 °C. A CCD was located 0.3 m downstream of the sample for monitoring the beam intensity and position in shot-by-shot. Scattering from the water was recorded using three MPCCDs with a pixel size of 50  $\mu$ m. The distance between the sample and the detector was 1 m. In this experimental setting, the speckle size on the detector plane is estimated to be 0.18 mm. As suggested by a recent study, an SDO with wavefront division has intrinsic reduction of speckle contrast due to the

difference in the speckle position on the detector plane.<sup>47</sup> In the current setting, the angular difference between two sub-pulses was expected to be 0.15 mrad, leading the differences in the speckle positions between two sub-pulses  $\sim 0.15$  m on the detector plane, which corresponds to 83 % of the speckle size. This angular mismatch would lead to a 74% decrease in speckle contrast. Because the contrast with a single pulse from the fixed-delay branch was 0.23 and that with uncorrelated beam was 0.12, the decreased contrast would be  $(0.23-0.12) \times 0.26 + 0.12 = 0.15$ , which is consistent with the measured values at  $\Delta t = 0$  ps, considering a further decrease due to the relative positional fluctuation of the sub-pulses.

## Data availability

Data supporting the findings of this study are available within the article or from the corresponding authors upon reasonable request.

## Figures

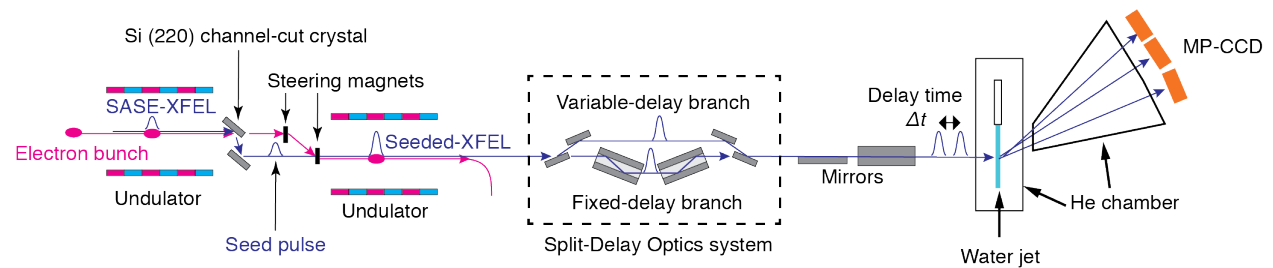


**Figure 1 | Experimental setting of XPCS using split-and-delay optics and reflection self-seeding at BL3, SACLA.**<sup>18</sup> The seed pulse was produced by monochromatizing the SASE from the upstream undulator segments. Then the seed was amplified in the downstream undulators. The details are described in ref.<sup>36</sup> The amplified X-ray pulse was split into two sub-pulses using

the SDO.<sup>31</sup> The sub-pulses with a delay time  $\Delta t$  are focused by mirrors<sup>40</sup> and hit the water jet. Scattered X-rays were recorded by the MP-CCDs.<sup>42</sup>

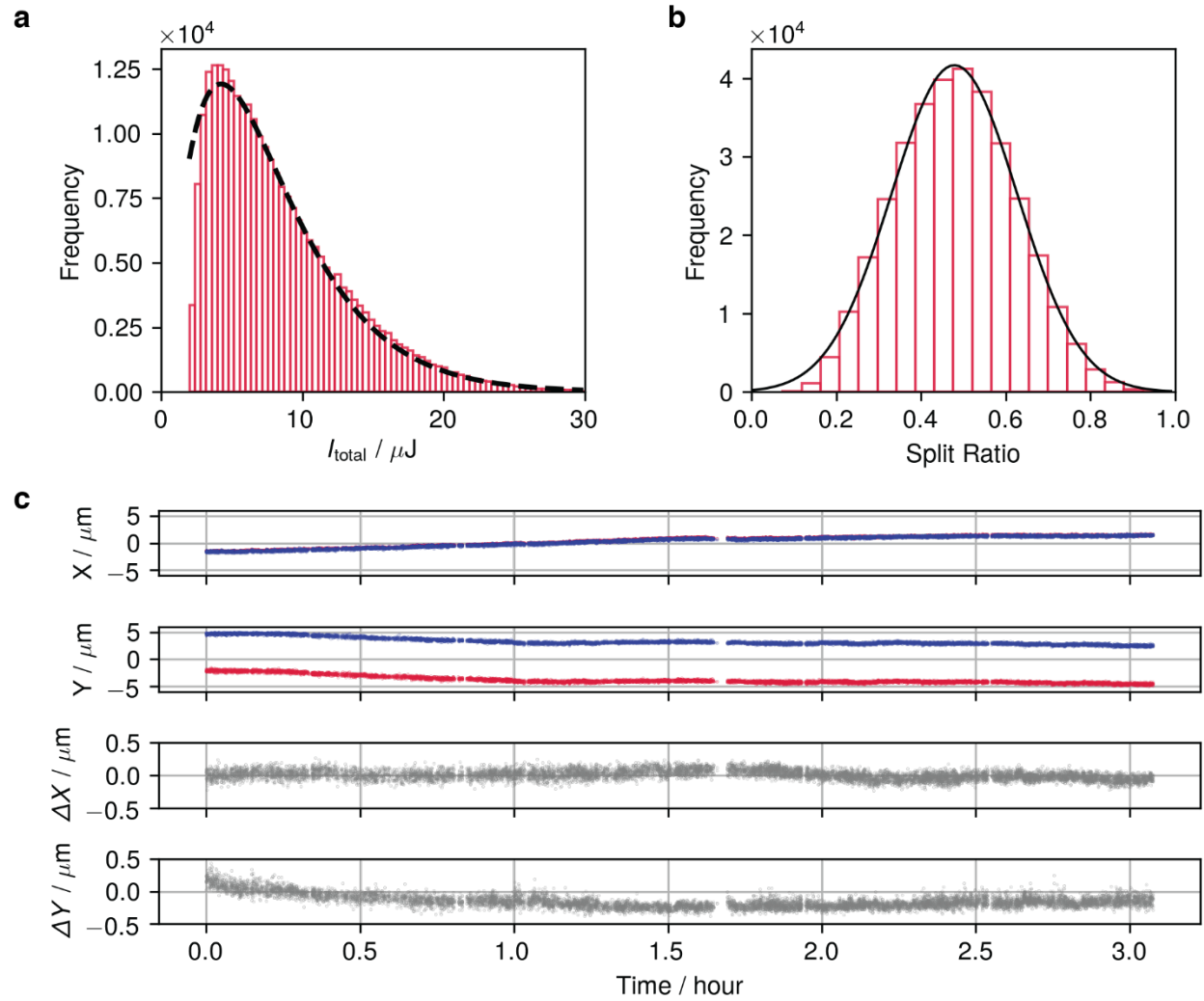


**Figure 2 | Statistics of self-seeded XFEL pulses after split-and-delay optics.** **a.** A pulse energy distribution at sample position for 280,815 shots (red bar). The dashed line represents the best fit to a gamma distribution. **b.** A histogram of the split ratio  $R$  for 340,732 shots. The solid line represents the best fit to a Gaussian distribution for the average = 0.48 and the standard deviation = 0.15. **c.** A time-course of X-ray beam position at the sample position. The position of two X-ray pulses was shifted in the  $Y$  direction to distinguish them.

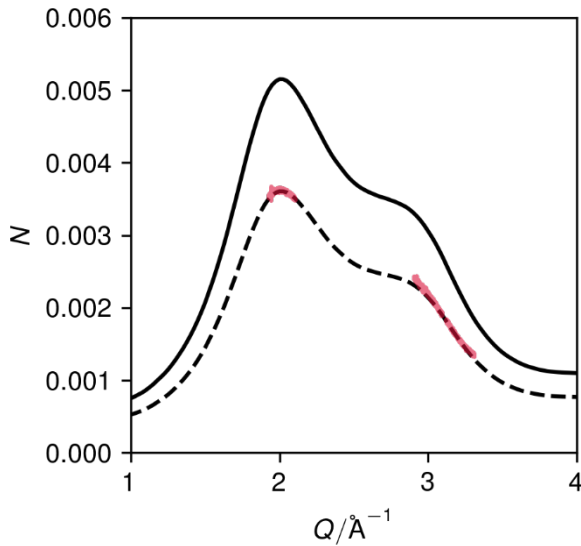


**Figure 3 | X-ray scattering from water.** The number of photons at each pixel per shot obtained by averaging 29,051 shots with  $\Delta t = 2.0$  ps (red lines). The area around  $Q = 2.0 \text{ \AA}^{-1}$  was covered by a single MPCCD and that around  $Q = 3.0 \text{ \AA}^{-1}$  was covered by a dual MPCCD.<sup>42</sup> The averaged incident pulse energy  $\langle I_{\text{tot}} \rangle$  was  $7.3 \text{ \mu J}$ . The solid black line is the estimation of X-ray elastic scattering using the result of high-energy X-ray diffraction intensity profile,<sup>44</sup> the thickness of sample, the X-ray energy, the size of pixel, and the average number of X-ray photon for a single shot. The dashed line is  $\times 0.7$  of the solid line.

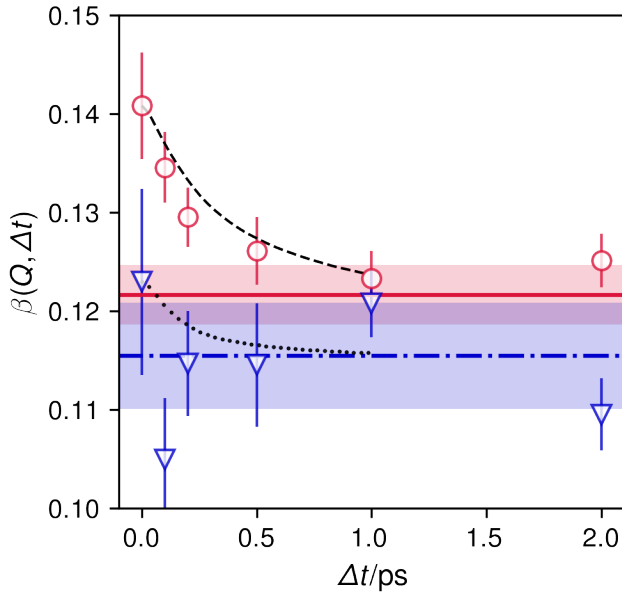


**Figure 4 | X-ray contrast obtained by maximum-likelihood estimation.** (Circles) At  $Q = 2.00 \pm 0.06 \text{ \AA}^{-1}$ . (Triangles) At  $Q = 3.00 \pm 0.04 \text{ \AA}^{-1}$ . The solid line ( $Q = 2.00 \pm 0.06 \text{ \AA}^{-1}$ ) and dot-dashed line ( $Q = 3.00 \pm 0.04 \text{ \AA}^{-1}$ ) represent the contrast measured when there was no overlap between two sub-pulses. The uncertainty was calculated using the second derivative of the log-likelihood based on the approach in reference<sup>20</sup> and the uncertainty for the solid and dot-dashed lines is represented by the shade. The dashed line and the dotted line are estimated by the result of inelastic X-ray scattering at  $Q = 2.00 \text{ \AA}^{-1}$  and  $3.00 \text{ \AA}^{-1}$ , respectively,<sup>45,46</sup> where their amplitude was set by the XPCS result at  $\Delta t = 0$ .

1. Sutton, M. *et al.* Observation of speckle by diffraction with coherent X-rays. *Nature* **352**, 608–610 (1991).
2. Stephenson, G. B., Robert, A. & Grübel, G. Revealing the atomic dance. *Nat. Mater.* **8**, 702–703 (2009).

3. Madsen, A., Fluerasu, A. & Ruta, B. Structural Dynamics of Materials Probed by X-Ray Photon Correlation Spectroscopy. in *Synchrotron Light Sources and Free-Electron Lasers* 1617–1641 (Springer, 2016).
4. Sutton, M. A review of X-ray intensity fluctuation spectroscopy. *Comptes Rendus Phys.* **9**, 657–667 (2008).
5. Grübel, G. & Zontone, F. Correlation spectroscopy with coherent X-rays. *J. Alloys Compounds* **362**, 3–11 (2004).
6. Dierker, S. B., Pindak, R., Fleming, R. M., Robinson, I. K. & Berman, L. X-Ray Photon Correlation Spectroscopy Study of Brownian Motion of Gold Colloids in Glycerol. *Phys. Rev. Lett.* **75**, 449–452 (1995).
7. Thurn-Albrecht, T. *et al.* Photon Correlation Spectroscopy of Colloidal Palladium Using a Coherent X-Ray Beam. *Phys. Rev. Lett.* **77**, 5437–5440 (1996).
8. Mochrie, S. G. J. *et al.* Dynamics of Block Copolymer Micelles Revealed by X-Ray Intensity Fluctuation Spectroscopy. *Phys. Rev. Lett.* **78**, 1275–1278 (1997).
9. Falus, P., Borthwick, M. A. & Mochrie, S. G. J. Fluctuation Dynamics of Block Copolymer Vesicles. *Phys. Rev. Lett.* **94**, 016105 (2005).
10. Caronna, C., Chushkin, Y., Madsen, A. & Cupane, A. Dynamics of Nanoparticles in a Supercooled Liquid. *Phys. Rev. Lett.* **100**, 055702 (2008).
11. Shinohara, Y., Kishimoto, H., Yagi, N. & Amemiya, Y. Microscopic Observation of Aging of Silica Particles in Unvulcanized Rubber. *Macromolecules* **43**, 9480–9487 (2010).
12. Leitner, M., Sepiol, B., Stadler, L.-M., Pfau, B. & Vogl, G. Atomic diffusion studied with coherent X-rays. *Nat. Mater.* **8**, 717–720 (2009).

13. Ruta, B. *et al.* Atomic-Scale Relaxation Dynamics and Aging in a Metallic Glass Probed by X-Ray Photon Correlation Spectroscopy. *Phys. Rev. Lett.* **109**, 165701 (2012).
14. Ruta, B. *et al.* Revealing the fast atomic motion of network glasses. *Nat. Commun.* **5**, 3939 (2014).
15. Baron, A. Q. R. High-Resolution Inelastic X-Ray Scattering I: Context, Spectrometers, Samples, and Superconductors. in *Synchrotron Light Sources and Free-Electron Lasers* (eds. Jaeschke, E. J., Khan, S., Schneider, J. R. & Hastings, J. B.) 1643–1719 (Springer International Publishing, 2016).
16. Stone, M. B. *et al.* A comparison of four direct geometry time-of-flight spectrometers at the Spallation Neutron Source. *Rev. Sci. Instrum.* **85**, 045113 (2014).
17. Emma, P. *et al.* First lasing and operation of an ångstrom-wavelength free-electron laser. *Nat. Photon.* **4**, 641–647 (2010).
18. Ishikawa, T. *et al.* A compact X-ray free-electron laser emitting in the sub-ångström region. *Nat. Photon.* **6**, 540–544 (2012).
19. Osaka, T. *et al.* Wavelength-tunable split-and-delay optical system for hard X-ray free-electron lasers. *Opt. Express* **24**, 9187 (2016).
20. Roseker, W. *et al.* Towards ultrafast dynamics with split-pulse X-ray photon correlation spectroscopy at free electron laser sources. *Nat. Commun.* **9**, 1704 (2018).
21. Grübel, G., Stephenson, G. B., Gutt, C., Sinn, H. & Tschentscher, Th. XPCS at the European X-ray free electron laser facility. *Nucl. Instrum. Meth. Phys. Res. B* **262**, 357–367 (2007).
22. Gutt, C. *et al.* Measuring temporal speckle correlations at ultrafast x-ray sources. *Opt. Express* **17**, 55 (2009).

23. Dixon, P. K. & Durian, D. J. Speckle Visibility Spectroscopy and Variable Granular Fluidization. *Phys. Rev. Lett.* **90**, 184302 (2003).
24. Bandyopadhyay, R., Gittings, A. S., Suh, S. S., Dixon, P. K. & Durian, D. J. Speckle-visibility spectroscopy: A tool to study time-varying dynamics. *Rev. Sci. Instrum.* **76**, 093110 (2005).
25. Inoue, I., Shinohara, Y., Watanabe, A. & Amemiya, Y. Effect of shot noise on X-ray speckle visibility spectroscopy. *Opt. Express* **20**, 26878 (2012).
26. Li, L. *et al.* Photon statistics and speckle visibility spectroscopy with partially coherent X-rays. *J. Synchrotron Rad.* **21**, 1288–1295 (2014).
27. Verwohlt, J. *et al.* Low Dose X-Ray Speckle Visibility Spectroscopy Reveals Nanoscale Dynamics in Radiation Sensitive Ionic Liquids. *Phys. Rev. Lett.* **120**, 168001 (2018).
28. Perakis, F. *et al.* Coherent X-rays reveal the influence of cage effects on ultrafast water dynamics. *Nat. Commun.* **9**, 1917 (2018).
29. Hara, T. *et al.* Two-colour hard X-ray free-electron laser with wide tunability. *Nat. Commun.* **4**, 2919 (2013).
30. Marinelli, A. *et al.* High-intensity double-pulse X-ray free-electron laser. *Nat. Commun.* **6**, 6369 (2015).
31. Hirano, T. *et al.* Performance of a hard X-ray split-and-delay optical system with a wavefront division. *J. Synchrotron Rad.* **25**, 20–25 (2018).
32. Sakamoto, J. *et al.* Design of a prototype split-and-delay unit for XFEL pulses, and their evaluation by synchrotron radiation X-rays. *J. Synchrotron Rad.* **24**, 95–102 (2017).
33. Roseker, W. *et al.* Performance of a picosecond x-ray delay line unit at 8.39 keV. *Opt. Lett.* **34**, 1768 (2009).

34. Roseker, W. *et al.* Development of a hard X-ray delay line for X-ray photon correlation spectroscopy and jitter-free pump–probe experiments at X-ray free-electron laser sources. *J. Synchrotron Rad.* **18**, 481–491 (2011).
35. Roseker, W. *et al.* Double-pulse speckle contrast correlations with near Fourier transform limited free-electron laser light using hard X-ray split-and-delay. *Sci. Rep.* **10**, 5054 (2020).
36. Inoue, I. *et al.* Generation of narrow-band X-ray free-electron laser via reflection self-seeding. *Nat. Photon.* **13**, 319–322 (2019).
37. Emma, C. *et al.* Experimental demonstration of fresh bunch self-seeding in an X-ray free electron laser. *Appl. Phys. Lett.* **110**, 154101 (2017).
38. Amann, J. *et al.* Demonstration of self-seeding in a hard-X-ray free-electron laser. *Nat. Photon.* **6**, 693–698 (2012).
39. Tono, K. *et al.* Single-shot beam-position monitor for x-ray free electron laser. *Rev. Sci. Instrum.* **82**, 023108 (2011).
40. Yumoto, H. *et al.* Focusing of X-ray free-electron laser pulses with reflective optics. *Nat. Photon.* **7**, 43–47 (2013).
41. Goodman, J. W. *Statistical Optics*. (John Wiley & Sons, 1984).
42. Kameshima, T. *et al.* Development of an X-ray pixel detector with multi-port charge-coupled device for X-ray free-electron laser experiments. *Rev. Sci. Instrum.* **85**, 033110 (2014).
43. Hruszkewycz, S. O. *et al.* High Contrast X-ray Speckle from Atomic-Scale Order in Liquids and Glasses. *Phys. Rev. Lett.* **109**, 185502 (2012).

44. Skinner, L. B. *et al.* Benchmark oxygen-oxygen pair-distribution function of ambient water from x-ray diffraction measurements with a wide  $Q$ -range. *J. Chem. Phys.* **138**, 074506 (2013).
45. Shinohara, Y. *et al.* Viscosity and real-space molecular motion of water: Observation with inelastic x-ray scattering. *Phys. Rev. E* **98**, 022604 (2018).
46. Iwashita, T. *et al.* Seeing real-space dynamics of liquid water through inelastic x-ray scattering. *Sci. Adv.* **3**, e1603079 (2017).
47. Sun, Y. *et al.* Realizing split-pulse x-ray photon correlation spectroscopy to measure ultrafast dynamics in complex matter. *Phys. Rev. Research* **2**, 023099 (2020).
48. Gelman, A. Prior distributions for variance parameters in hierarchical models (comment on article by Browne and Draper). *Bayesian Anal.* **1**, 515–534 (2006).

## Acknowledgments

X-ray scattering work by Y. Shinohara, W.D., C.W.R., and T.E. was supported by U.S. Department of Energy, Office of Science, Office of Basic Energy Science, Division of Materials Sciences and Engineering. Work by T.O. was supported by JSPS KAKENHI (Grant No. 18K18307) and work by I.I. was supported by JSPS KAKENHI (Grant No. 19K20604). The experiments at SACLA were carried out under the approval of JASRI (Proposal No. 2018B8041, 2019A8043, and 2019B8011).